RSC Advances

PAPER

View Article Online
View Journal | View Issue

Cite this: *RSC Adv.*, 2019, **9**, 29549

Flower-like Bi_2S_3 nanostructures as highly efficient anodes for all-solid-state lithium-ion batteries†

Pooja Kumari,[ab] Kamlendra Awasthi,[b] Shivani Agarwal,[c] Takayuki Ichikawa,[ad] Manoj Kumar *[b] and Ankur Jain *[d]

Received 4th July 2019
Accepted 6th September 2019

DOI: 10.1039/c9ra05055h

rsc.li/rsc-advances

Herein, we introduce the detailed electrochemical reaction mechanism of Bi_2S_3 (bulk as well as nanostructure) as a highly efficient anode material with Li-ions in an all-solid-state Li-ion battery (LIB). Flower-like Bi_2S_3 nanostructures were synthesized by a hydrothermal method and were used as an anode material in a LIB with $LiBH_4$ as a solid electrolyte. The X-ray diffraction (XRD) pattern verified the formation of Bi_2S_3 nanostructures, which belongs to the orthorhombic crystal system (JCPDS no. 00-006-0333) with the *Pbnm* space group. Morphological studies confirmed the flower-like structure of the obtained product assembled from nanorods with the length and diameter in the range of 150–400 nm and 10–150 nm respectively. The electrochemical galvanostatic charge–discharge profile of these nanostructures demonstrates exciting results with a high discharge and charge capacity of 685 mA h g^{-1} & 494 mA h g^{-1} respectively at 125 °C. The discharge and charge capacities were observed as 375 mA h g^{-1} and 352 mA h g^{-1} after 50 cycles (with 94% coulombic efficiency), which are much better than the cells having bulk Bi_2S_3 as the anode material.

Introduction

The growth of portable electronic devices and hybrid electric vehicles (HEVs) has generated an increased demand for batteries with large gravimetric capacity and high volumetric capacity as the power sources. In this regard, rechargeable lithium-ion batteries (LIBs) have been studied intensively because they can provide a large capacity and high power as compared to other batteries. In particular, alloying type anode materials with a larger capacity than that of commercial graphite anodes have been investigated actively as possible alternative anode materials.[1–3] Belonging to this family, bismuth (Bi) has attracted considerable attention as an anode material with a gravimetric capacity of 386 mA h g^{-1}, which is comparable to the graphite anode (372 mA h g^{-1}). In addition, its 4 fold higher volumetric capacity (3800 mA h cm^{-3}) as compared to carbon makes it a promising material, since the volumetric capacity is as important as the gravimetric capacity for practical applications with a need of less space but large capacity. Although there have been several studies on Bi as an anode material with liquid electrolytes, it still suffers from poor electrochemical performance.[4–7] However, Huang *et al.* used graphene encapsulated Bi@C-TiO_x as anode with liquid electrolyte and obtained a superior Li-ion storage electrochemical performance, where ultra large graphene (which work as "silk magic carpet") interfacial layer provided a highly conductive path for fast charge transfer along with low volume expansion during discharge/charge measurements.[8] A similar cushioning effect was also observed in our recent report where a hydride based solid electrolyte – $LiBH_4$ was used with Bi (as an anode) to assemble an all-solid-state battery and the obtained results showed that the existence of $LiBH_4$ as well as acetylene black (AB) impressively improved the cyclability of Bi anode.[9]

In order to further enhance the capacity, Bi based chalcogenides (Bi_2X_3; X = S, Se, Te) have been explored, as the element X has ability to alloy with Li.[10,11] Out of these chalcogenides, Bi_2S_3 possesses highest capacity and in addition to Li-ion batteries it has been widely used in many fields, such as optics,[12,13] photoelectricity,[14,15] photocatalysis[16,17] and biology[18,19] due to its direct band gap (1.3 eV). Bi_2S_3 has been proposed as an ideal host for hydrogen[20,21] and Li[22,23] because of its unique lamellar structure. Layered bismuth sulfide (Bi_2S_3) has emerged as an important type of Li-storage material due to its high theoretical gravimetric capacity (625 mA h g^{-1} – 2 times that of carbon), volumetric capacity (4250 mA h cm^{-3} – 5 times that of carbon) and intriguing reaction mechanism. Although Bi_2S_3 has many advantages including high capacity, nontoxic nature and low cost, it's practical application is hindered by the poor cycling stability due to its large volumetric expansion.[24] Bi_2S_3 nanorods recorded a high discharge

[a]*Graduate School of Engineering, Hiroshima University, Higashi-Hiroshima 739-8527, Japan*

[b]*Department of Physics, Malaviya National Institute of Technology, Jaipur, Rajasthan-302017, India. E-mail: kmanujk@gmail.com*

[c]*Department of Physics, JECRC University, Jaipur, Rajasthan-303905, India*

[d]*Natural Science Centre for Basic Research and Development, Hiroshima University, Higashi-Hiroshima 739-8521, Japan. E-mail: ankur.j.ankur@gmail.com*

† Electronic supplementary information (ESI) available. See DOI: 10.1039/c9ra05055h

capacity of 810 mA h g^{-1} as reported by Zhou *et al.*, however, they did not investigate the charge capacity and cycling stability.[25] Later the Li-storage capability of dandelion-like Bi_2S_3 microspheres was investigated by Zhang *et al.* and unfortunately, the capacities declined very rapidly and retained a value of only 100 mA h g^{-1} after 8 cycles.[26] Similarly, Ma *et al.* investigated the Li-storage capability of uniform Bi_2S_3 fabrics, which showed the initial discharge and charge capacities of 1083 and 652 mA h g^{-1} respectively, however, the capacity dropped to 366 mA h g^{-1} after 10 cycles.[27] The major issue in storing Li-ions in Bi_2S_3 is poor cyclability, which is strongly associated with their reaction towards lithium. Jung *et al.* have investigated the reaction mechanism between Bi_2S_3 and Li-ion and the results showed that the conversion step presented a high volumetric expansion (90%) with 74% volume increment in subsequent alloying contribution. Such a huge volume variations upon lithiation and de-lithiation caused severe particle cracking and pulverization, which broke the electrical contacts in the anode, leading to a drastic capacity fading.[24] Thus, improvement of the cyclability of the Bi_2S_3 materials remains a key challenge to be addressed. In addition to it, another big safety issue also exists for practical applications, which is related to the use of flammable liquid electrolytes. So based on the above key problems, firstly, we replaced the liquid electrolyte by a solid electrolyte ($LiBH_4$) as a solution to the safety issue and secondly, investigated the electrochemical reaction mechanism between Bi_2S_3 and Li-ion in all-solid-state Li-ion battery.

Herein, hydrothermally synthesized Bi_2S_3 nanoflowers are used as anode material in all-solid-state battery, since the flowerlike structure may provide higher number of electrochemical reaction sites than other nanostructures, which can significantly improve the Li-storage performance of Bi_2S_3.[26,28] In order to compare the electrochemical performance and improvement by using nano-size anode, commercial bulk Bi_2S_3 has also been used as active material in the anode. The cycling performance is also reported in this work.

Experimental

Synthesis of Bi_2S_3 nanoflowers

Bi_2S_3 nanoflowers were prepared through the hydrothermal method.[29] To prepare the nanoflowers, 0.61 g high purity (99.99%) bismuth nitrate pentahydrate ($Bi(NO_3)_3 \cdot 5H_2O$) and 0.25 g thiourea (Tu) were dissolved into 60 ml deionized water and stirred at 250 rpm for 1 h to form a homogeneous solution. This stirred solution was transferred into a Teflon lined autoclave with a capacity of 100 ml. The autoclave was then sealed and heated at 140 °C for 2 h. The autoclave was cooled down to room temperature after the chemical reaction. The resulting black color precipitate was collected using filtration and washed with deionized water and ethanol several times, then dried at room temperature before characterizations.

Materials characterizations

The surface morphology of the prepared nanostructures was observed using field emission scanning electron microscopy (FEI Nova SEM 450) and transmission electron microscopy (FEI Technai G20). The X-ray diffraction (XRD) using a Rigaku-RINT 2500 diffractometer equipped with Cu Kα radiation, was performed on all the materials used in this work, to observe the crystalline structure and purity of the samples. The surface morphology of the negative electrode before and after electrochemical cycling was also recorded using SEM (JEOL, JSM-6380A). All of the sample handlings were carried out in a high purity Ar-filled glove box, to protect them from atmospheric exposure.

Coin cell fabrication and electrochemical measurements

The negative electrode (anode) composite material was prepared by ball-milling of Bi_2S_3 nanoflowers (as prepared)/ Bi_2S_3 (as received, Sigma Aldrich with 99% purity), $LiBH_4$ and acetylene black (AB) in 40 : 30 : 30 weight ratio for 2 h with 1 h milling and 30 min rest pattern under Ar atmosphere. 10 SS balls were used at 370 rpm in Fritsch P7 milling machine, for the preparation of the 200 mg anode composite material. $LiBH_4$ and acetylene black were dried under vacuum heating at 200 °C for 24 h before using them for milling. To investigate the Li-storage properties of prepared anode composite material, a coin cell was assembled with Li-foil as counter electrode and $LiBH_4$ as a solid electrolyte. To fabricate the cell, a three-layer pellet was prepared having Li-foil (thickness of 0.1 mm) on SS plate as first layer (layer thickness $\sim$ 0.62 mm), $LiBH_4$ as second layer (layer thickness $\sim$ 0.68 mm) and anode composite powder as third layer (layer thickness $\sim$ 0.01–0.03 mm). The detailed information is given elsewhere.[8] The prepared three-layer pellet was placed in a coin cell and was packed using perfluoroalkoxy (PFA) gasket. A charge–discharge analyzer (HJ1001SD8, Hokuto Denko Co.) was used to observe the electrochemical performance of Bi_2S_3 *vs.* Li-metal, by galvanostatic charge–discharge measurements at an optimized rate of 0.1C [ESI Fig. S1–S6†]. All the electrochemical measurements in this report were performed at 125 °C, to obtain the fast Li^+ conduction through $LiBH_4$.[30]

Results and discussion

Fig. 1(A) indicates the XRD patterns of synthesized nanostructured Bi_2S_3 sample. All the diffraction peaks can be indexed to an orthorhombic Bi_2S_3 phase (JCPDS card no. 00-006-0333) with *Pbnm* space group along with some Bi_2O_3 traces. The structural analysis of the obtained Bi_2S_3 pattern designates the lattice parameters as $a = 11.15$ Å, $b = 11.30$ Å and $c = 3.9810$ Å, agreeing well with the JCPDS database values. Since morphology plays an important role in electrochemical performance, it is essential to assess the morphology of the prepared sample which was done using FESEM and TEM measurements and the images are illustrated in Fig. 1(B). The FESEM image (Fig. 1B-a) depicts the flower-like pattern and also exhibits that each shoot in this pattern is formed along a well-arranged assembly between many nanorods. The nanorods have a variation in the diameter between 10–150 nm with the length in the range of 150–400 nm. All the prepared samples were further characterized by TEM, as shown in Fig. 1B-b. TEM image of the

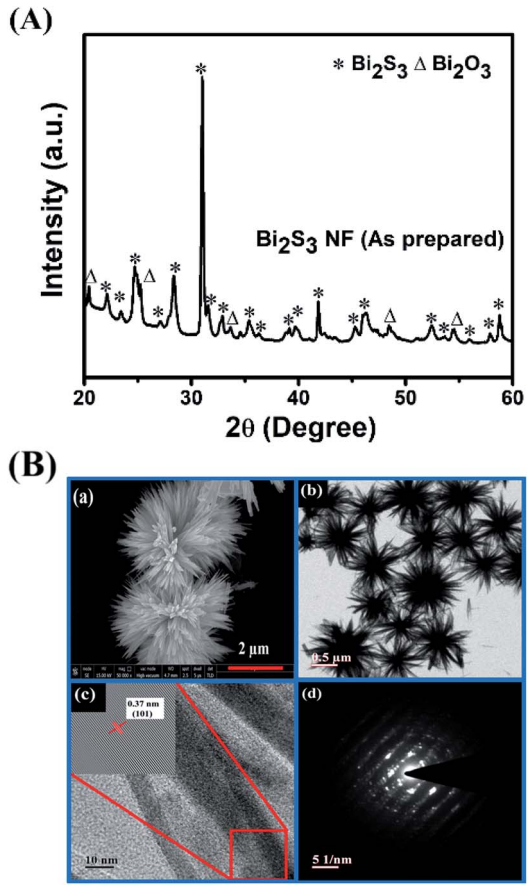

Fig. 1 (A) XRD pattern of as prepared Bi_2S_3 nanoflowers (B) FE-SEM & TEM images of Bi_2S_3 nanoflowers (a, b) HRTEM & SAED images of nanoflowers (c & d).

prepared nanostructures confirms the above FESEM observations and designates that the flower like morphology was successfully obtained. Fig. 1B-c depicts the HRTEM observations of the prepared nanostructure, in which the lattice fringes show interplanar spacing of 0.37 nm, allocated to the (101) plane of Bi_2S_3. SAED pattern of nanoflowers indicates the polycrystalline nature as shown in Fig. 1B-d.

The first galvanostatic discharge–charge curve of the nano Bi_2S_3–$LiBH_4$ composite anode material is illustrated in Fig. 2, which was performed at 125 °C temperature with the 0.1C current rate. The current rate of 0.1C was optimized by performing several discharge–charge curves at different C-rates (Fig. S1–S3†). The prepared nanostructures recorded the first discharge and charge capacities as 685 mA h g^{-1} (corresponding volumetric capacity: 4644 mA h cm^{-3}) and 1330 mA h g^{-1} respectively, in the voltage window of 0.2–2.5 V. The obtained first lithiation capacity is slightly higher than the theoretical capacity (625 mA h g^{-1}) of Bi_2S_3; it may be associated to the contribution of carbon (AB), which is contained in the anode composite material in sufficient amount (30 wt%). On the other hand, the first charge capacity is found much higher, approximately 2 fold higher than the discharge capacity. This indicates the existence of side reaction during the de-lithiation process.

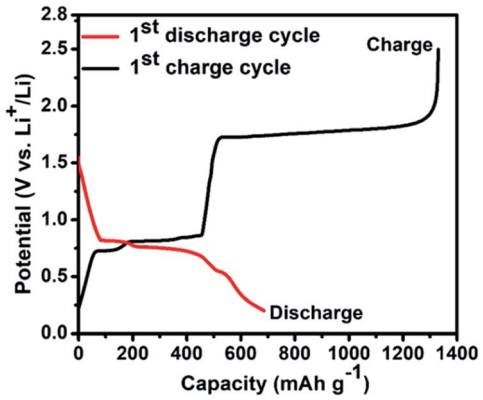

Fig. 2 First galvanostatic discharge–charge profile of the nano Bi_2S_3–$LiBH_4$ composite anode material in the voltage range of 0.2–2.5 V at 125 °C with the rate of 0.1C.

The de-lithiation process at around 1.7 V transforms Li_2S to S, however, this freshly generated sulfur can thermochemically react with $LiBH_4$ (component of anode composite material), thus again forming Li_2S. This thermochemically generated Li_2S again takes part in the electrochemical reaction and releases Li ion. This cyclic process continues until the full consumption of $LiBH_4$. The calculated value of charge capacity (according to the existing amount of $LiBH_4$ and Bi_2S_3 in anode composite) as per above speculation agrees well with the obtained capacity during de-lithiation. The consumption of $LiBH_4$ due to this thermochemical reaction should affect the Li ion mobility through the anode material in successive cycles, which is visible during the discharging charging cycling (Fig. S4†). The capacity is drastically reduced to around 200 mA h g^{-1} within 12 cycle and finally the cell stopped working in 13th cycle. The above mechanism is also supported from the morphological observation of the anode surface after the cycles, where the cracks and crumbling are clearly observed (Fig. S5†). These cracks also confirm the above proposed thermochemical reaction.

To avoid this thermochemical reaction, the galvanostatic discharge/charge cycling test was performed on nano Bi_2S_3–$LiBH_4$ composite electrode in a limited potential window 0.2–1.5 V at 125 °C temperature with 0.1C rate, and the results are illustrated in Fig. 3. The composite electrode material affords the initial discharge and charge capacities of 685 mA h g^{-1} and 494 mA h g^{-1}, respectively, with 95.8% coulombic efficiency. The discharge and charge capacities dropped to 532 mA h g^{-1} and 502 mA h g^{-1} in the second cycle and then decreased steadily to 375 mA h g^{-1} (*ca.* 2543 mA h cm^{-3}) and 352 mA h g^{-1} in 50th number of cycles. The obtained capacities are considerably better or comparable to a variety of other Bi_2S_3 nanostructures.[26,27] After the cycling test of composite electrode material, SEM was also performed to observe the surface condition of the negative electrode. No cracks or crumbling on the surface of anode material are observed even after 50 cycles (Fig. S6†), in contrast to the case of cycling between 0.2–2.5 V when these appeared only after 13 cycles. Even though the thermochemical reaction restricts us to perform the de-lithiation/lithiation cycles in a limited potential window of

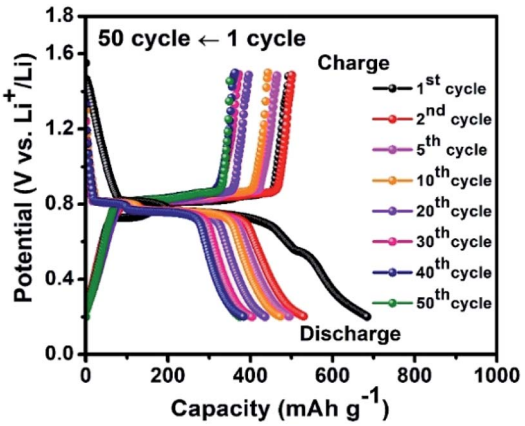

Fig. 3 Cyclic performance of the nano Bi_2S_3–$LiBH_4$ composite anode material in the voltage range of 0.2–1.5 V at 125 °C with 0.1C.

0.2–1.5 V, the prepared nano Bi_2S_3–$LiBH_4$ composite negative electrode showed the good cyclic stability over 50 cycles with no surface damage.

In order to observe the superiority of nanostructures over bulk Bi_2S_3, commercial bulk Bi_2S_3 (Sigma Aldrich, 99% purity) was also used as anode material with $LiBH_4$ as solid electrolyte. For the electrochemical characterizations, the anode composite material using above Bi_2S_3 powder was prepared by ball milling using similar method as described above for nanostructures based composite anode material. To observe the electrochemical performance of bulk sample, galvanostatic discharge and charge characterization was performed on the assembled coin cell at 125 °C within the potential window 0.2–2.5 V with the rate of 0.1C.

Fig. 4(a) exhibits the first galvanostatic discharge–charge profile of bulk Bi_2S_3–$LiBH_4$ composite anode material and the obtained discharge capacity of the prepared anode is recorded as 617 mA h g^{-1} (volumetric capacity: 4183 mA h cm^{-3}) whereas the first charge capacity is found to be 1145 mA h g^{-1}. The values are slightly less as compared to those of nanoflowers of Bi_2S_3. However, the higher charge capacity than the discharge capacity follows the same trend as nanoflowers. It is noteworthy here that the presence of small amount of Bi_2O_3 in the prepared nanoflowers of Bi_2S_3 doesn't affect the reaction mechanism as the nature of electrochemical profile (*i.e.* plateau voltage, shape *etc.*) is quite similar for both the composites. To explain the mechanism behind the obtained high charge capacity and plateaus, *ex situ* XRD was performed at the selected potentials which are identified as numbers in Fig. 4(a).

The XRD pattern of the prepared composite anode material with as purchased bulk Bi_2S_3, AB and heat treated $LiBH_4$ is shown in Fig. 4b. It is observed that a mechanochemical reaction took place during the milling as evident from the presence of Bi and Li_2S peaks in addition to the starting material *i.e.* Bi_2S_3 & $LiBH_4$. Since a mechanochemical reaction between Bi_2S_3 and $LiBH_4$ was observed during the milling, XRD experiment has also been performed after 1 h heating (which is kept before all the experiments in order to stabilize the temperature) at 125 °C in oil bath before starting the discharging process, which is indicated by point 1 at

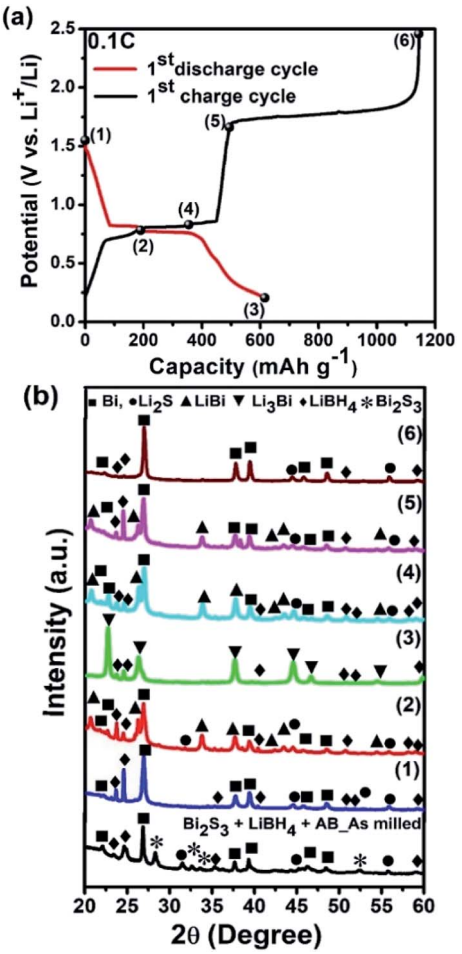

Fig. 4 (a) The first galvanostatic discharge–charge curves for bulk Bi_2S_3–$LiBH_4$ composite anode material in the voltage range of 0.2–2.5 V at 0.1C. (b) *Ex situ* XRD profiles of Bi_2S_3–$LiBH_4$ composite anode material evolution upon the first electrochemical discharge–charge process at different stages.

1.56 V in Fig. 4a. The obtained XRD pattern (point 1) gives information about the reduction reaction of Bi_2S_3 to Bi and Li_2S (Fig. 4b). Thus, the starting material Bi_2S_3 is completely transformed to Bi and Li_2S due to thermochemical and mechanochemical reaction during the 1 h heating and milling process respectively. This is in line with the non-existence of expected 1st discharge plateau at around 1.6 V (Fig. 4a). The second plateau is appeared at 0.79 V which corresponds to the alloying reaction of Bi with Li to form LiBi as suggested by XRD profile at point 2. Further discharge down to 0.2 V (point 3) proceeded through the lithiation of Bi and LiBi to form Li_3Bi (plateau at 0.75 V), which is confirmed from the XRD pattern of the discharging point 3. Similar discharge plateau position corresponding to the alloying process of Li_3Bi was observed by Z. D. Huang *et al.*[8] In the reverse scan *i.e.* during charging, these two plateaus are again observed corresponding to lithium extraction from Li_3Bi to form LiBi and then to form Bi at around ~0.82 V, which is evident from XRD at point 4 and point 5. Some peaks corresponding to LiBi are also visible at point 5, but the major phase is Bi and Li_2S. The XRD experiment at point 6 was performed after charging the coin cell up to 2.5 V, which also showed the existence

of Bi and Li_2S rather than the starting material *i.e.* Bi_2S_3. This finding strengthens our above speculation of thermochemical reaction between $LiBH_4$ and freshly produced sulfur from Li_2S. In addition, the peaks corresponding to $LiBH_4$ are also visible in all the patterns as it is presented as a solid electrolyte in addition to anode composite material.

The existence of the thermochemical reaction of the Bi_2S_3–$LiBH_4$ composite anode material could also be experienced by cyclic voltammetry (CV) experiment. Fig. 5 shows the CV curves for the bulk Bi_2S_3 as well as nanoflowers between 0.2–2.5 V at a scan rate of 0.1 mV s^{-1}. The open circuit voltage (OCV) of the bulk and nano composite electrode material based cell was 1.56 V and 1.55 V, respectively. In the first cathodic scan of the bulk sample, a slightly weak peak at 1.42 V may be ascribed to the Li_2S formation, while the peaks at 0.79 V and 0.72 V are due to the formation of LiBi followed by Li_3Bi phase. On the other hand, the reverse anodic scan process shows two peaks at around 0.85 V and 0.88 V corresponding to the de-lithiation of Li_3Bi to LiBi and Bi respectively. Further de-lithiation gave rise to a broad peak with a lot of noise between 1.86–2.01 V, which should correspond to the transformation of Li_2S to S. However, the noise in this region suggested the possibility of additional reaction along with the electrochemical reaction. The similar behavior was observed in the case of nano Bi_2S_3 also. The first cathodic peak at 1.45 V is weaker than the bulk sample, which is quite obvious due to the kinetically fast thermochemical reaction between $LiBH_4$ and nano Bi_2S_3 in comparison with bulk Bi_2S_3 during initial 1 h heating, thus converting nano Bi_2S_3 to Li_2S in more amount. The other peaks found were quite similar to that of bulk Bi_2S_3. On the basis of the above findings, *i.e.*, first galvanostatic discharge–charge analysis, XRD analysis, and CV profiles, the reversible reaction mechanism can be depicted as follows:

$$Bi_2S_3 + 6Li \leftrightarrow 3Li_2S + 2Bi + Li \leftrightarrow 3Li_2S + Bi + LiBi + 5Li \leftrightarrow 3Li_2S + 2Li_3Bi \quad (1)$$

Fig. 6a shows the cyclic galvanostatic discharge charge profiles at 0.1C up to 50 cycles in between 0.2–1.5 V. The first discharge and charge capacities were found to be 662 mA h g^{-1} and 524 mA h g^{-1}, respectively and dropped to 586 mA h g^{-1} and 485 mA h g^{-1} respectively in the subsequent second cycle, which further reduced down to 311 mA h g^{-1} and 225 mA h g^{-1} in 50th cycle respectively. In order to compare the cyclic performance, a curve between the capacity *vs.* cycle number is plotted and is shown in Fig. 6b. It is clearly evident that the initial capacity of bulk sample is slightly higher than nano composite anode material, however, the cyclic stability of the nano Bi_2S_3–$LiBH_4$ composite anode material is found to be much better than bulk Bi_2S_3–$LiBH_4$ composite electrode. The nano Bi_2S_3–$LiBH_4$ composite anode material shows only 29.5% capacity decay from the first capacity, which is much lower than 47% capacity decay of bulk Bi_2S_3–$LiBH_4$ composite electrode. The possible reasons for the better stability of nanoflowers may include high surface area and excellent charge transfer kinetics of the nanostructures due to shorter diffusion path.

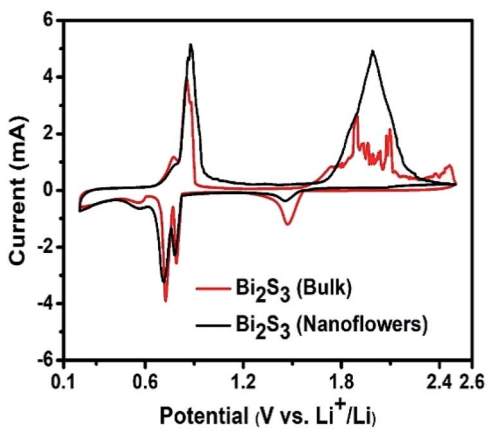

Fig. 5 Cyclic voltammograms of Bi_2S_3 (bulk & nanoflowers)–$LiBH_4$ composite anode material scanned at 0.1 mV s^{-1}.

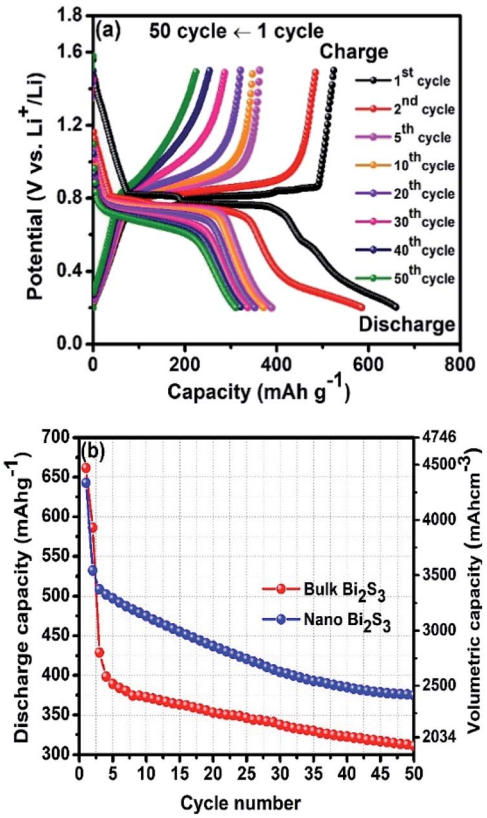

Fig. 6 (a) Cyclic performance of the bulk Bi_2S_3–$LiBH_4$ composite anode material in the voltage range of 0.2–1.5 V at 125 °C with 0.1C. (b) Cyclic stability (capacity *vs.* no. of cycle) of commercial bulk Bi_2S_3 and Bi_2S_3 nanoflowers.

Conclusions

In summary, the nanoflowers of Bi_2S_3 have shown nice and stable electrochemical performance in all solid state Li-ion battery. The discharge and charge capacities were found to be 375 mA h g^{-1} and 352 mA h g^{-1}, respectively, for nanoflowers in comparison to 311 mA h g^{-1} and 225 mA h g^{-1}, respectively, for

bulk Bi_2S_3 composite anode material after 50 cycles. The values are much higher than the previous reports. The electrochemical reaction mechanism lithiation/de-lithiation of Bi_2S_3 is established using XRD experiments during the discharging and charging experiment. As per our best knowledge, this is the first report on Bi_2S_3 (as an anode) with $LiBH_4$ (as a solid electrolyte) in all-solid-state LIB. An interesting thermochemical reaction between sulfur and $LiBH_4$ was observed during charging process, which compelled us to limit the potential window between 0.2–1.5 V. Despite this limited potential window, we attained higher stability and capacity for our Li-ion battery in comparison with previously reported results. This problem can be overcome in future by enabling the use of $LiBH_4$ at lower temperature or by using other sulfide based electrolytes. The exciting cyclic performance with high capacity, demonstrates the potential of Bi_2S_3 to be used as novel electrode material for Li-ion batteries and $LiBH_4$ as a solid electrolyte.

Conflicts of interest

There are no conflicts to declare.

Acknowledgements

This work was financially supported by DST, New Delhi (IFA-13/PH-84), SERB, New Delhi (ECR/2016/1780, ECR/2016/1888) and UGC-DAE CSR, Indore (CSR-IC-MSRSR-23/CRS-231/2017-18/1312, CSR-IC/CRS-73/2014-15/581).

References

1 Y. Idota, T. Kubota, A. Matsufuji, Y. Maekawa and T. Miyasaka, Tin-Based Amorphous Oxide: A High – Capacity Li-Ion Storage Material, *Science*, 1997, **276**, 1395–1397.

2 B. M. Winter, J. O. Besenhard, M. E. Spahr and P. Novak, Insertion Electrode Materials for Rechargeable Lithium Batteries, *Adv. Mater.*, 1998, **10**, 725–763.

3 I.-S. Kim, G. E. Blomgren and P. N. Kumta, Nanostructured Si/TiB_2 Composite Anodes for Li-Ion Batteries, *Electrochem. Solid-State Lett.*, 2003, **6**, A157–A161.

4 C. Julien and I. Samaras, Studies of Lithium Insertion in Bismuth Chalcogenides Compounds, *Solid State Ionics*, 1989, **36**, 113–120.

5 W. Xianming, T. Nishina and I. Uchida, Lithium alloy formation at bismuth thin layer electrode and its kinetics in propylene carbonate electrolyte, *J. Power Sources*, 2002, **104**, 90–96.

6 Y. Nuli, J. Yang and M. Jiang, Synthesis and characterization of Sb/CNT and Bi/CNT composite as anode materials for lithium-ion batteries, *Mater. Lett.*, 2008, **62**, 2092–2095.

7 C. M. Park, S. Yoon, S. Il Lee and H. J. Sohn, Enhanced electrochemical properties of nanostructured bismuth-based composites for rechargeable lithium batteries, *J. Power Sources*, 2009, **186**, 206–210.

8 Z. D. Huang, H. Lu, K. Qian, Y. W. Fang, Q. C. Du, Y. B. He, T. Masese, X. S. Yang, Y. W. Ma and W. Huang, Interfacial engineering enables Bi@C-TiOx microspheres as superpower and long life anode for lithium-ion batteries, *Nano Energy*, 2018, **51**, 137–145.

9 P. Kumari, K. Sharma, P. Pal, M. Kumar, T. Ichikawa and A. Jain, Highly efficient & stable Bi & Sb anodes using lithium borohydride as solid electrolyte in Li-ion batteries, *RSC Adv.*, 2019, **9**, 13077–13081.

10 F. Tu, J. Xie, G. Cao and X. Zhao, Self-Assembly of Bi_2Te_3 Nanoplate/Graphene-Nanosheet Hybrid by One-Pot Route and Its Improved Li-Storage Properties, *Materials*, 2012, **5**, 1275–1284.

11 J. Ni, X. Bi, Y. Jiang, L. Li and J. Lu, Bismuth chalcogenide compounds Bi_2X_3 (X = O, S, Se): applications in electrochemical energy storage, *Nano Energy*, 2017, **34**, 356–366.

12 G. Chen, Y. Yu, K. Zheng, T. Ding, W. Wang, Y. Jiang and Q. Yang, Fabrication of ultrathin Bi_2S_3 nanosheets for high-performance, flexible, visible-NIR photodetectors, *Small*, 2015, **11**, 2848–2855.

13 G. Konstantatos, L. Levina, J. Tang and E. H. Sargent, Sensitive solution processed Bi_2S_3 nanocrystalline photodetector, *Nano Lett.*, 2008, **8**, 4002–4006.

14 A. K. Rash, M. Bernechea, L. Martinez and G. Konstantatos, Solution-Processed Heterojunction Solar Cells Based on p-type PbS Quantum Dots and n-type Bi_2S_3 Nanocrystals, *Adv. Mater.*, 2011, **23**, 3712–3717.

15 D. Becerra, M. T. S. Nair and P. K. Nair, Analysis of a Bismuth Sulfide/Silicon Junction for Building Thin Film Solar Cells, *J. Electrochem. Soc.*, 2011, **158**, 741–749.

16 Ch. Tang, Y. Zhang, J. Su, C. Wang, R. Sun, J. Zhang and G. Li, Synthesis and photocatalytic properties of vertically aligned Bi_2S_3 Platelets, *Solid State Sci.*, 2016, **51**, 24–29.

17 J. Chen, S. Qin, G. Song, T. Xiang, F. Xin and X. Yin, Shape-controlled solvothermal synthesis of Bi_2S_3 for photocatalytic reduction of CO_2 to methyl formate in methanol, *Dalton Trans.*, 2013, **42**, 15133–15138.

18 Y. Fang, C. Peng, R. Guo, L. Zheng, J. Qin, B. Zhou, M. Shen, X. Lu, G. Zhang and X. Shi, Dendrimer-stabilized bismuth sulfide nanoparticles: synthesis, characterization, and potential computed tomography imaging applications, *Analyst*, 2013, **138**, 3172–3180.

19 J. Liu, X. Zheng, L. Yan, L. Zhou, G. Tian, W. Yin, L. Wang, Y. Liu, Z. Hu, Z. Gu, C. Chen and Y. Zhao, Bismuth sulfide nanorods as a precision nanomedicine for in vivo multimodal imaging-guided photothermal therapy of tumor, *ACS Nano*, 2015, **9**, 696–707.

20 Q. Wang, X. Wang, W. Lou and J. Hao, Ionothermal synthesis of bismuth sulfide nanostructures and their electrochemical hydrogen storage behavior, *New J. Chem.*, 2010, **34**, 1930–1935.

21 B. Zhang, X. Ye, W. Hou, Y. Zhao and Y. Xie, Biomolecule-Assisted Synthesis and Electrochemical Hydrogen Storage of Bi_2S_3 Flowerlike Patterns with Well-Aligned Nanorods, *J. Phys. Chem. B*, 2006, **110**, 8978–8985.

22 Y. Zhao, T. Liu, H. Xia, L. Zhang, J. Jiang, M. Shen, J. Ni and L. Gao, Branch-structured Bi_2S_3–CNT hybrids with improved

lithium storage capability, *J. Mater. Chem. A*, 2014, **2**, 13854–13858.

23 Y. Zhao, D. Gao, J. Ni, L. Gao, J. Yang and Y. Li, One-pot facile fabrication of carbon-coated Bi_2S_3 nanomeshes with efficient Li-storage capability, *Nano Res.*, 2014, **7**, 765–773.

24 H. Jung, C. M. Park and H. J. Sohn, Bismuth sulfide and its carbon nanocomposite for rechargeable lithium-ion batteries, *Electrochim. Acta*, 2011, **56**, 2135–2139.

25 H. Zhou, S. Xiong, L. Wei, B. Xi, Y. Zhu and Y. Qian, Acetylacetone-Directed Controllable Synthesis of Bi_2S_3 Nanostructures with Tunable Morphology, *Cryst. Growth Des.*, 2009, **9**, 3862–3867.

26 Z. Zheng, C. Zhou, H. Lu, M. Jia, Y. Lai and J. Li, Facile synthesis of dandelion-like Bi_2S_3 microspheres and their electrochemical properties for lithium-ion batteries, *Mater. Lett.*, 2013, **91**, 100–102.

27 J. Ma, Z. Liu, J. Lian, X. Duan, T. Kim, P. Peng, X. Liu, Q. Chen, G. Yao and W. Zheng, Ionic liquids-assisted synthesis and electrochemical properties of Bi_2S_3 nanostructures, *CrystEngComm*, 2011, **13**, 3072–3079.

28 R. Jin, G. Li, Z. Zhang, L. X. Yang and G. Chen, Carbon coated flowerlike Bi_2S_3 grown on Ni foam as binder free electrodes for electrochemical hydrogen and Li-ion storage capacities, *Electrochim. Acta*, 2015, **173**, 458–464.

29 C. J. Tang, Y. X. Zhang, X. C. Dou and G. H. Li, Seed-assistant hydrothermal synthesis of 3D Bi_2S_3 mat like architecture, *J. Cryst. Growth*, 2010, **312**, 692–697.

30 M. Matsuo and S. Orimo, Lithium Fast-Ionic Conduction in Complex Hydrides: Review and Prospects, *Adv. Energy Mater.*, 2011, **1**, 161–172.